Optoelectronic transport through quantum Hall edge states

2015 New J. Phys. 17 023007

(http://iopscience.iop.org/1367-2630/17/2/023007)

New Journal of Physics
The open access journal at the forefront of physics

Deutsche Physikalische Gesellschaft DPG
IOP Institute of Physics

Published in partnership with: Deutsche Physikalische Gesellschaft and the Institute of Physics

OPEN ACCESS

RECEIVED
24 September 2014

REVISED
21 November 2014

ACCEPTED FOR PUBLICATION
31 December 2014

PUBLISHED
30 January 2015

PAPER

Optoelectronic transport through quantum Hall edge states

C Kastl[1,2], M Stallhofer[1,2], D Schuh[3], W Wegscheider[4] and A W Holleitner[1,2]

[1] Walter Schottky Institut and Physik-Department, Technische Universität München, Am Coulombwall 4a, D-85748 Garching, Germany
[2] Nanosystems Initiative Munich (NIM), Schellingstr. 4, D-80799 München, Germany
[3] Institut für Experimentelle und Angewandte Physik, Universität Regensburg, D-93040 Regensburg, Germany
[4] Laboratorium für Festkörperphysik, ETH Zürich, Schafmattstrasse 16, 8093 Zürich, Switzerland

E-mail: holleitner@wsi.tum.de

Keywords: quantum hall edge states, quantum points contacts, optolectronics

Abstract

We use GaAs-based quantum point contacts as mesoscopic detectors to locally analyze the flow of photogenerated electrons in a two-dimensional electron gas (2DEG) at perpendicular, quantizing magnetic fields. The 2DEG is formed within a quantum well of a doped GaAs/AlGaAs-hetero-structure. We find an optoelectronic signal along the lateral boundaries of the 2DEG, which is consistent with an optically induced quantum transport through quantum Hall edge channels. We demonstrate that photogenerated electrons can be directly injected into an edge channel, transported across several tens of micrometers and read-out on-chip by the quantum point contact.

1. Introduction

The spatial current distribution within a two-dimensional electron gas (2DEG) in the quantum Hall regime has been under debate since the discovery of the integer quantum Hall effect in 1980 by Klitzing *et al* [1–3]. The commonly used edge channel picture emphasizes the importance of the sample boundaries [4, 5]. It stands in contrast to publications concentrating on conduction paths within the bulk. Trugman *et al* proposed a current which is transported by extended states within the bulk by a percolation of localized states [6], and there are explanations of the quantum Hall effect by small electric field gradients in the sample without the need for edge channels [7]. As introduced by Chklovskii *et al*, edge channels can be further distinguished into compressible and incompressible regions [8].

Over the years, there have been many approaches to visualize the edge channels. Early experiments used optical techniques such as photoresistance mapping [9] and Hall photovoltage imaging [10, 11] with a spatial resolution on the order of micrometers. By contrast, subsequent scanning probe experiments allowed imaging down to the nanometer-scale. In particular, implementing a scanning force technique [12], Weitz *et al* and Ahlswede *et al* succeeded in detecting the potential drop in the incompressible stripes [13, 14]. The regions between the incompressible regions show no detectable potential drop, as expected for a compressible electron gas. As predicted by theory [8], the bulk region becomes incompressible at integer filling factors. Scanning gate microscopy [15, 16] uses a tip as a gate to deplete the electron gas locally and thereby to influence the resistance. At integer filling factors, the 2DEG is insensitive to such a local gate, whereas at non-integer filling factors this technique can be used to gain information on the percolation transition of edge states and their mutual coupling. The compressible regions have been visualized by a scanning capacitance detection [17, 18]. By additionally implementing a single electron transistor as local detector, both edge channels [19–21] as well as localized states [22] were resolved. Other techniques, such as scanning tunneling spectroscopy [23], microwave impedance microscopy [24], and local thermometry [25], provided further insights into the nature of the integer as well as fractional quantum Hall edge states [26–28], such as the real space distribution of wave function and conductivity as well as the interplay of heat and charge transport in the 2DEG. Most of the reports on the quantum Hall edge states describe experiments without optical excitation (e.g. [12–28]). For experiments with an optical excitation [9–11], the role and the interplay of photogenerated electrons and holes have not been discussed in the context of the photoinduced transport through the quantum Hall edges states. To this end, we

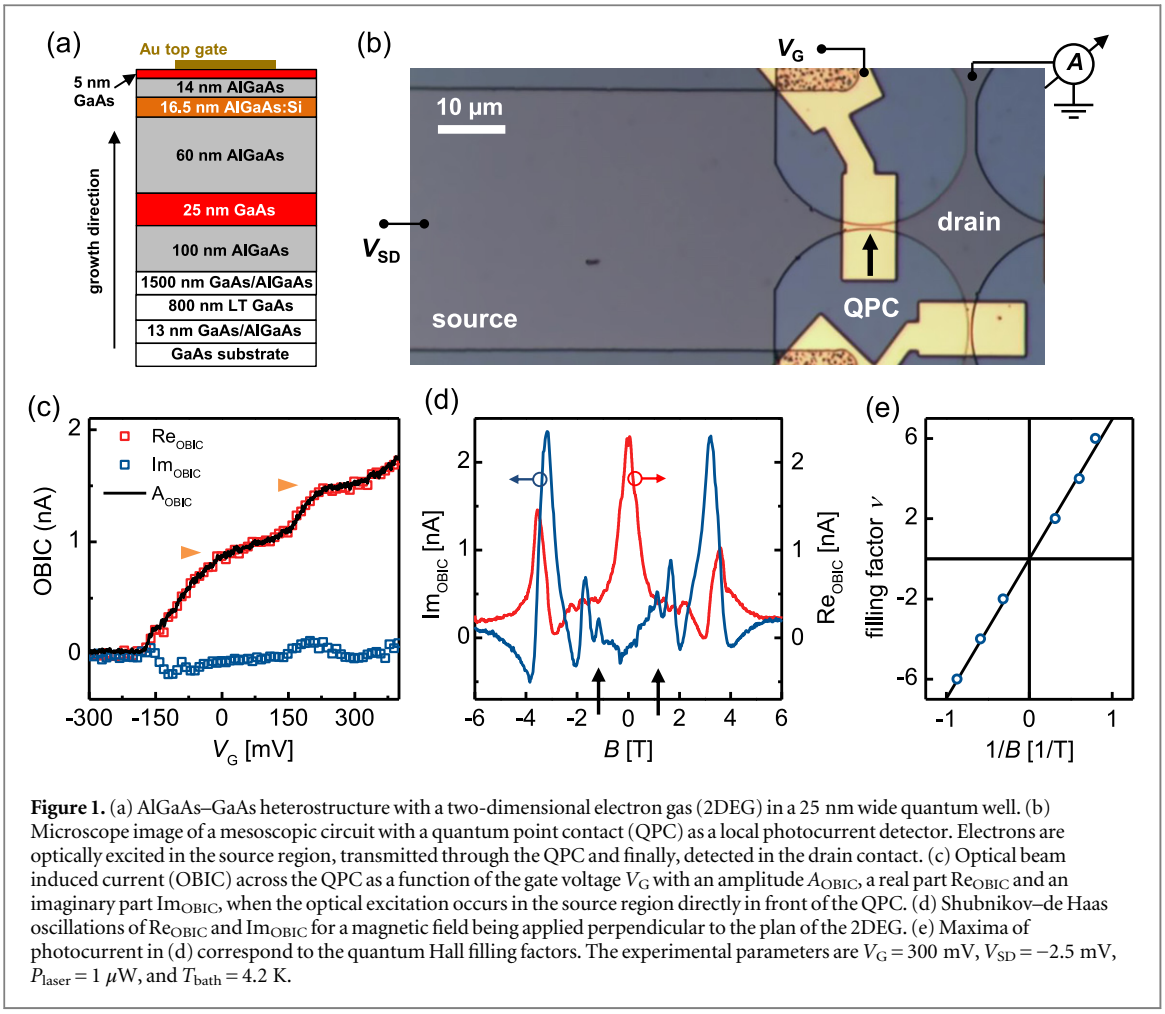

Figure 1. (a) AlGaAs–GaAs heterostructure with a two-dimensional electron gas (2DEG) in a 25 nm wide quantum well. (b) Microscope image of a mesoscopic circuit with a quantum point contact (QPC) as a local photocurrent detector. Electrons are optically excited in the source region, transmitted through the QPC and finally, detected in the drain contact. (c) Optical beam induced current (OBIC) across the QPC as a function of the gate voltage V_G with an amplitude A_{OBIC}, a real part Re_{OBIC} and an imaginary part Im_{OBIC}, when the optical excitation occurs in the source region directly in front of the QPC. (d) Shubnikov–de Haas oscillations of Re_{OBIC} and Im_{OBIC} for a magnetic field being applied perpendicular to the plan of the 2DEG. (e) Maxima of photocurrent in (d) correspond to the quantum Hall filling factors. The experimental parameters are $V_G = 300$ mV, $V_{SD} = -2.5$ mV, $P_{laser} = 1$ μW, and $T_{bath} = 4.2$ K.

experimentally investigate the photoinduced transport through quantum Hall edge states in an on-chip manner. We excite edge states by a focused laser and detect the corresponding photocurrent signal by the help of a quantum point contact (QPC) as a local photocurrent detector. We demonstrate that at high magnetic fields, where Landau-quantization applies, a dominant photocurrent signal shows up at the edges of such a circuit. The sign of the photocurrent at the edges depends on the polarity of the magnetic field, as it is consistent with an optically induced quantum transport dominated by edge states. We identify two mechanisms of photocurrent generation in this regime. First, photogenerated electrons are directly injected into the quantum Hall edge states. Second, charge carriers are photogenerated in the vicinity of an edge state and they capacitively influence the transport through it. Both mechanisms explain our findings in the framework of charge carrier transport within one-dimensional quantum Hall edge states to the QPC detector. We determine the characteristic photocurrent length within an edge channel to be several tens of micrometer. This length substantially exceeds the mean free path of photogenerated charge carriers at zero and small magnetic fields [29, 30]. Our experiments suggest that the measured length is limited by the effective diffusion length of the photogenerated holes which capacitively control the photocurrent detection at the QPC. In the light of recent, novel material systems, such as topological insulators [31–33], where edge channel conduction applies, our results may proof essential for a read-out-scheme of the optoelectronic properties of corresponding circuits.

2. Radio frequency scanning photocurrent microscopy

Starting point is an AlGaAs/GaAs-heterostructure with a 25 nm wide GaAs quantum well 95 nm below the surface (figure 1(a)). An AlGaAs: Si-doping layer with a width of 16 nm is located 19 nm below the surface. In turn, the quantum well comprises a 2DEG with Fermi energy $E_{Fermi} = 9.8$ meV and electron mobility of $\mu = 1.7 \times 10^6$ cm^2 V^{-1} s^{-1}. The latter translates into an elastic mean free path of $l_{mfp} = 15$ μm at $T = 4.2$ K. In photoluminescence experiments, the optical transition energy from the valence to the conduction band of the quantum well including E_{Fermi} is determined to be $E = 1.543$ eV. A two-dimensional mesa is formed by optical lithography. One-dimensional QPCs are defined by electron beam lithography and a subsequent wet etching

process with an etch depth of about 85 nm [34–37]. The two 2DEG regions adjacent to a QPC are connected to a voltage source (V_{SD}) and to a current voltage amplifier, respectively (figure 1(b)). An opaque gold gate on top of the QPC is connected to a gate voltage V_G which serves to adjust the electronic one-dimensional subbands of the QPC with respect to the Fermi energy of the 2DEG. Using a confocal scanning laser microscope with a spatial resolution of ~900 nm, we excite electron–hole pairs in the source region of the circuit and measure the resulting photocurrent from source to drain across the QPC with standard lock-in techniques. We excite at $E_{photon} = 1.550$ eV with $\Delta E_{FWHM} = 8$ meV, such that the photocurrent response is maximum, yet the excitation into the second two-dimensional subband of the quantum well can be neglected [29, 30].

The QPC acts as a spatially narrow and energetically sensitive detector of the photogenerated electrons propagating from source to drain [38]. Varying the trigger frequencies, different dynamics of the photocurrent become accessible. For a trigger frequency in the kHz-regime, the optical beam induced current (OBIC) is dominated by the photoconductive gain effect, which relies on the capacitive coupling of the photogenerated holes to the electronic subbands of the QPCs. The kHz (millisecond) scale relates to the recombination dynamics of spatially separated electrons and holes in the vicinity of the QPC [35, 39, 40]. In order to largely suppress these slow processes, we measure at 40.9 MHz which is the repetition frequency of the pulsed laser with a pulse duration $\tau_{FWHM} < 100$ ps. The overall electronic response time can be estimated to be $\tau_{RC} = R_{QPC} \cdot C \sim 0.5\ \mu$s, with $R_{QPC} \sim (2e^2/h)^{-1} \sim 12.5\ k\Omega$ the dominating resistance of the QPC, h the Planck constant, e the electron charge, and the capacitance $C \sim 40$ pF of the used coaxial lines. In principle, this timescale inhibits a high frequency detection of photogenerated electrons in the source region. However, as was demonstrated in [38], a repetition frequency in the MHz regime allows to detect processes induced by electrons, which are photogenerated in source and which then, tunnel across the QPC into drain. This can be understood in a way that the drain region is connected to the read-out circuit without the high impedance of the mesoscopic circuit. For instance, the radio frequency technique allows resolving the propagation length of mesoscopic photocurrents in a 2DEG which is dominated by electron–electron scattering processes [29, 30].

Figure 1(c) depicts the amplitude A_{OBIC} of the photocurrent signal at 40.9 MHz across the QPC (black line), for the laser being focused at a centered position 5 μm from the QPC in the source region. As a function of V_G, one can detect steps in A_{OBIC} (triangles), which relate to the one-dimensional subbands of the QPC [38, 42, 43]. The photocurrent signal comprises both an imaginary part Im_{OBIC} and a real part Re_{OBIC}, with $A_{OBIC} = \sqrt{\left(Im_{OBIC}\right)^2 + \left(Re_{OBIC}\right)^2}$. The red (blue) data in figure 1(c) depict Re_{OBIC} (Im_{OBIC}) of the radio frequency photocurrent response across the QPC. Spurious signals and parasitic effects, such as coherent pick-up or the capacitance of the wiring, are corrected by leveling Re_{OBIC} and Im_{OBIC} when the QPC pinches-off at negative V_G. The precise phase relation is given by the interplay of the capacitances as well as the resistances of both the 2DEG regions and the one-dimensional QPC. It changes with the application of a magnetic field B and the adjustment of the Fermi level in the circuit. Figure 1(d) depicts Im_{OBIC} and Re_{OBIC} as a function of B for the laser being focused at a centered position 5 μm from the QPC in the source contact. The magnetic field is applied perpendicularly to the plane of the 2DEG. For $|B| \leqslant \sim 0.5$ T, Re_{OBIC} dominates the signal. As discussed in detail in [30], this low-magnetic field regime can be understood by classical cyclotron orbits of the photogenerated electrons in combination with a predominant influence of electron–electron scattering processes. In this regime, the QPC detects the photogenerated, non-equilibrium electrons as they tunnel from source to drain. With increasing magnetic field, the trajectories of the photogenerated electrons in the source region are less commensurate with the etched, lateral aperture of the QPC and its finite width [30]. This explains why Re_{OBIC} decreases for increasing magnetic fields in the range of $|B| \leqslant \sim 0.5$ T. Consistently, the gate voltage dependence at zero magnetic field (figure 1(c)) demonstrates that the signal A_{OBIC} is dominated by Re_{OBIC} and that Im_{OBIC} is rather negligible.

The situation changes as soon as the Landau quantization dominates at higher magnetic fields. As indicated by arrows in figure 1(d), it is Im_{OBIC} which exhibits much clearer Shubnikov–de Haas oscillations with a distinct maximum at $B \approx \pm 3.2$ T. We interpret this change of the QPC detection scheme by an increasing influence of the capacitive coupling between the edge states in the source and the drain regions. Still, however, tunneling of photogenerated electrons across the QPC occurs, because Re_{OBIC} is finite even at the highest magnetic fields. The occurrence of Shubnikov–de Haas oscillations in Re_{OBIC} and Im_{OBIC} clearly demonstrates that the involved densities of states are described by a Landau-fan. This interpretation is consistent with earlier reports [44, 45] which show that the maxima in the density of states are directly related to maxima in the capacitance of a 2DEG in the quantum Hall regime. Starting with $\nu = 2$ for the most pronounced maximum at $B \approx 3.2$ T, we can assign spin-degenerate filling factors to the peaks in the photocurrent signal (figure 1(e)). The extracted total electron density of $n_{2D} = (1.68 \pm 0.04) \times 10^{11}$ cm^{-2} comprises both electrons due to doping (n_0) and optically induced charge carriers (n_{opt}). For the as-grown wafer, the electron density is determined to be $n_0 = 2.75 \times 10^{11}$ cm^{-2} measured without optical excitation. We attribute the difference between n_{2D} and n_0 to a degradation of the

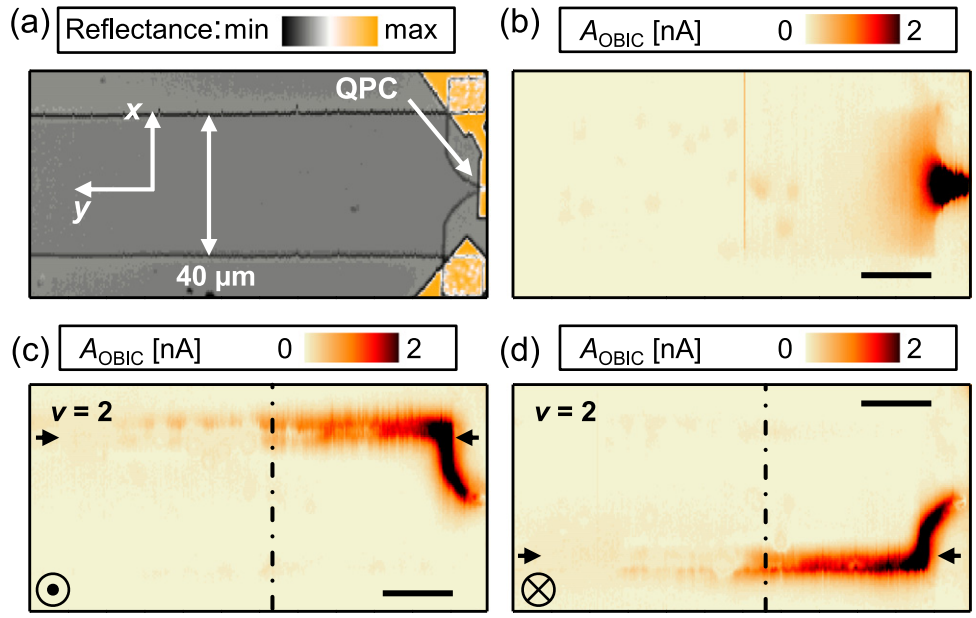

Figure 2. (a) Reflectance map of the source region (left) with the adjacent QPC (right). (b) Corresponding photocurrent map at $B = 0$ T. The photocurrent amplitude decays exponentially with distance to the QPC [29]. (c), (d) Photocurrent map at filling factor $\nu = 2$ with the magnetic field pointing outwards (inwards) w.r.t. the 2DEG plane. Photocurrent signal extends along the edge of the circuit with edge states propagating from source to drain. Scale bars are 20 μm. Color scale is clipped for improved contrast. The experimental parameters are $V_G = 300$ mV, $V_{SD} = -5$ mV, $P_{laser} = 1$ μW, and $T_{bath} = 4.2$ K.

heterostructure caused by the nanofabrication steps and numerous cooling cycles. In the following, we use the term filling factor with reference to the photocurrent properties as determined in figure 1(e).

3. Photoinduced quantum transport in one-dimensional edge channels

We record two-dimensional photocurrent maps for different magnetic fields. Figure 2(a) shows a reflectance map of the source region while the laser is scanned across it. The edges of the circuit appear dark, whereas the top gates appear bright. The arrow with two endings highlights the width of the mesa. On the right, the mesa edges forming the QPC are visible. At $B = 0$ T, the photocurrent amplitude A_{OBIC} is maximum near the QPC and it decays exponentially along the y-direction with a characteristic decay length of $\delta_{decay} = 6.3$ μm (figure 2(b)). This decay and the transport of the photogenerated electrons are consistent with a momentum relaxation limited, quasi-ballistic propagation from the excitation spot to the QPC. Therefore, δ_{decay} is in the same order as l_{mfp} for the lowest excitation intensities, as discussed in detail in [29].

At large magnetic fields, where the Landau quantization applies, the electronic transport can be described by one-dimensional, perfectly conducting edge states [4, 5]. If the Fermi energy is located in-between two Landau levels, the density of states at the Fermi energy is zero. Local variations of the Fermi energy result in elongated states along equipotential lines. These states are either localized around potential variations in the bulk or delocalized along the sample edge. According to [5], the latter states connect to the contacts. Consistently, at $\nu = 2$, we find a photocurrent signal that extends along the edge of the circuit even if the laser is positioned more than 50 μm away from the QPC (figures 2(c) and (d)). This length significantly exceeds l_{mfp} and δ_{decay} at zero magnetic field; a finding which already points towards an optoelectronic quantum transport regime. In figure 3(a), we depict line scans of the imaginary part Im_{OBIC} and the real part Re_{OBIC} of the complex photocurrent signal perpendicular to the 2DEG boundary (along the dashed-dotted line in figure 2(c)). The signal dominantly appears on the upper 2DEG boundary (dashed line in figure 3(a)). At the opposite edge (dotted line in figure 3(a)), the signal is largely reduced. The reduction can be explained by the source–drain asymmetry of the detection scheme using a QPC [38]. When the magnetic field direction is changed by 180°, the dominating signal appears on the lower boundary of the 2DEG (figure 3(b), also compare figures 2(c) and (d)). Based on this reversal of the signal and the long spatial extension of the signal, we interpret the data in terms of a photoinduced transport along quantum Hall edge states. The dominating signal in figures 2(c) and (d) stems from a quantum transport leading from source, across the QPC, to drain, while the largely reduced signal on the opposite edges stems from transport from drain to source. We note that the latter smaller signal can be better seen in the data cuts given in figures 3(a) and (b). Interestingly, for a large enough signal-to-noise ratio, we can

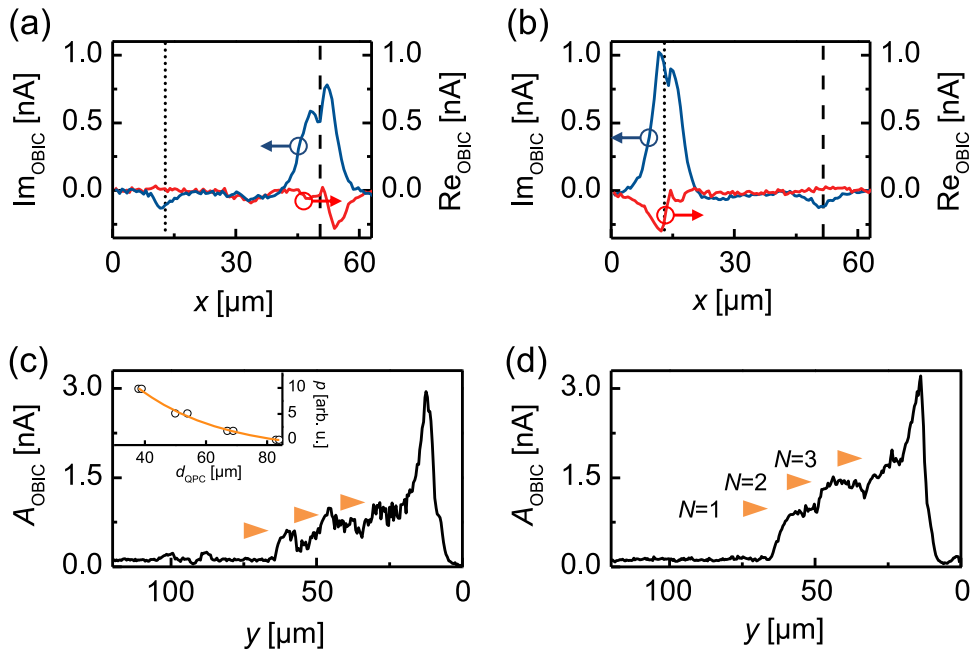

Figure 3. (a), (b) Photocurrent along dashed-dotted lines in figures 2(c), (d). Boundaries of the circuit are marked by a dotted and a dashed line. (c), (d) Photocurrent amplitude A_{OBIC} along lines indicated by arrows in figures 2(c), (d). Pronounced photocurrent steps (triangles) are related to one-dimensional subbands of the QPC. Inset in (c) shows the photoinduced shift of the Fermi-level within the QPC as a function of excitation position.

spatially resolve two major peaks in Im_{OBIC} at the edges of the 2DEG boundary. One peak is located inside and one peak is located outside the boundary of the 2DEG. To demonstrate this, the dotted and dashed lines in figures 3(a) and (b) highlight the boundaries of the 2DEG-mesa, as determined from reflectance measurements. Inside the 2DEG region, the peak can be attributed to an optical injection of charge carriers into the edge states. In the presentation of figures 3(a) and (b), the peak maximum occurs at a distance ~2 μm from the boundary, which is consistent with a calculated depletion width $l_d = 0.4$ μm due the upward bending of the conduction band at the boundary and a lateral spatial resolution of 0.9 μm. Outside the 2DEG region, where no GaAs-quantum well is present, an optical excitation at $E_{photon} = 1.55$ eV excites either in-gap states, e.g. within the AlGaAs tunneling barriers, or surface states within the etched area. Therefore, the observed photocurrent signal outside of the 2DEG region can be understood by a dominating capacitive coupling of the edge states within the 2DEG to these optically induced charges. The corresponding change of the Fermi level drives a current in the quantum Hall edge states. The observation of this capacitive photocurrent signal implies that the underlying time-scales are comparable to the measurement frequency ($1/f \sim 24$ ns). At low temperatures, the charge carrier recombination time in GaAs is in the subnanosecond regime [46], which would be too fast to explain the signal. However, this optical recombination time can be substantially longer even up to ~ms for trapped or spatially separated charge carriers [35, 40, 41].

We note that with the given signal-to-ratio, Re_{OBIC} has a minimum outside of the 2DEG region (figures 3(a) and (b)). A difference of Re_{OBIC} for an excitation inside and outside of the 2DEG agrees with the assumption of two different photocurrent mechanisms. We explain this detail of Re_{OBIC} by an increased electron density of the 2DEG when the laser is focused outside the 2DEG, as discussed in detail in section 5.

4. Influence of the photogenerated holes on the optoelectronic quantum transport

Generally speaking, the edge states should extend around the whole 2DEG-mesa of the source region. This raises the question of why the photocurrent signal declines with increasing distance to the QPC detector (figures 2(c) and (d)). We attribute the decreasing signal to a capacitive coupling of photogenerated holes to the one-dimensional subbands of the QPC-detector at the position of the QPC. In figures 3(c) and (d), we depict line scans parallel to the circuit boundary (arrows in figures 2(c) and (d)). The photocurrent amplitude A_{OBIC} decays step-like along the edge (y-direction) and finally vanishes for $y \approx 60$ μm. The step-like decay already indicates an impact of the photogenerated holes to one-dimensional subbands of the QPC via a photoconductive gain effect [35]. In other words, the photogenerated holes act as a quasi-gate voltage at the position of the QPC, and each step in figures 3(c) and (d) means that subbands $N = 1$, 2, and 3 dominate the detection scheme. The

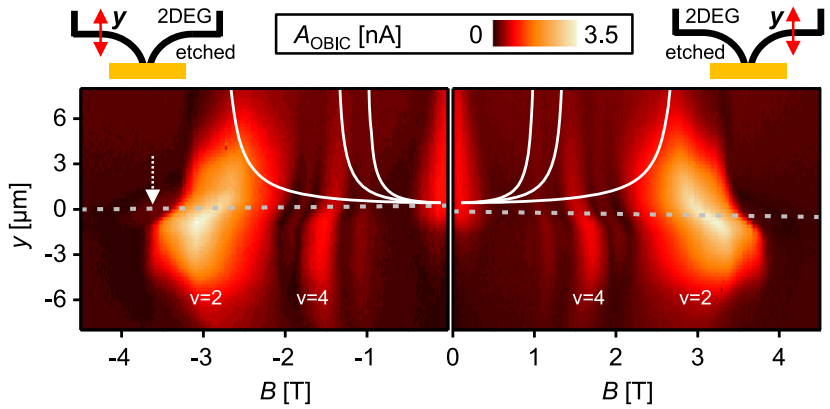

Figure 4. Photocurrent amplitude A_{OBIC} along a straight line across the sample boundary (as indicated schematically in the top insets) as a function of magnetic field. Solid lines mark theoretically expected position of incompressible strips. Dashed lines indicate sample boundary. Negative (positive) value of y corresponds to excitation outside (inside) 2DEG region. The experimental parameters are $V_G = 400$ mV, $V_{SD} = -2.5$ mV, $P_{laser} = 1$ μW, and $T_{bath} = 4.2$ K.

accumulation of photogenerated holes at the QPC is very likely, because the QPC constitutes a maximum of the valence band within the potential landscape of the overall circuit [35]. For an increasing distance of the excitation spot to the QPC, the effective hole diffusion length L_p limits the accumulated density of holes p at the QPC. Consequently, the number of occupied electronic subbands N in the QPC (triangles in figures 3(c) and (d)) is reduced, which ultimately limits the detection of the edge state transport. In a simplified model, we can estimate L_p assuming that p induces an electron density in the QPC as $\Delta n_{QPC} \propto p$, where the proportionality is given by the efficiency of the capacitive coupling. The number of quantization steps N in the photocurrent (number of occupied subbands in the QPC) indicates the photoinduced shift of the Fermi level within the QPC

$$p \propto \Delta n_{QPC} \propto \int_0^{E_N} \sum_N \mathrm{d}E \ \mathrm{DOS(E)}. \tag{1}$$

The inset in figure 3(c) shows the calculated hole density (in arbitrary units) as a function of distance d_{QPC} between the excitation position and the QPC. From this, we can estimate $L_p = 27$ μm $\pm$ 4 μm. The parameter L_p is an effective diffusion length because it obviously depends on the lifetime of the spatially separated, photogenerated electrons and holes in combination with the repetition frequency and the power of the laser, and on the applied voltages because the latter change the potential landscape of the circuit. However, the above estimate gives a conceptual insight into the influence of the photogenerated holes onto the overall optoelectronic response of the circuit.

5. Impact of compressible and incompressible strip formation

The self-consistent spatial rearrangement of the edge states results in the formation of conducting regions (compressible strips), which are separated by insulating regions (incompressible strips) [8, 47]. The kth insulating incompressible dipolar strip forms within the 2DEG at a distance $\Delta \mathrm{d_k}$ from the boundary of the 2DEG

$$\Delta d_k = \frac{l_d}{1 - (k/\nu)^2}, \tag{2}$$

with ν the bulk filling factor and $l_d = \frac{4V\varepsilon\varepsilon_0}{\pi e n_s}$ the width of the depletion layer. The confining potential V can be approximated by half of the bandgap of GaAs due to the mid-gap Fermi-level pinning at the surface [48]. To investigate the impact of the compressible and incompressible strips in our optoelectronic experiments, we scan the laser across the sample boundary (upper panel of figure 4) and record the photocurrent A_{OBIC} as a function of position y and magnetic field B. The dashed line indicates the sample boundary as extracted from a simultaneous reflectance measurement. A negative (positive) value of y corresponds to an excitation outside (inside) the 2DEG region. Again, we find two distinct photocurrent responses; one for an excitation inside and one for an excitation outside of the 2DEG region. The peaks of A_{OBIC} at approximately $B \approx 1.8$ T and $B \approx 3$ T correspond to filling factors $\nu = 4$ and $\nu = 2$. We find that the Shubnikov–de-Haas oscillations are shifted towards larger magnetic fields for an excitation outside of the 2DEG region compared to inside. The shift corresponds to an increased electron density in the 2DEG of $\Delta n_{2DEG} = 0.2 \times 10^{11}$ cm^{-2}. This finding is consistent with an earlier report [40], that photogenerated charge carriers outside an etched GaAs/AlGaAs-mesa capacitively increase the

Fermi level inside a doped quantum well of the mesa. In particular, the capacitively induced shift is maximum when the laser is positioned slightly outside of the 2DEG boundaries. The arrow in figure 4 highlights this finding. When the laser is scanned away from this position, either outside or inside the 2DEG, the additionally induced electron density $\Delta n_{2\mathrm{DEG}}$ decreases. As a consequence, we detect a shift of the photocurrent resonances towards smaller magnetic fields. Hereby, one can understand the variation of $\mathrm{Re}_{\mathrm{OBIC}}$ at the 2DEG boundaries, as discussed in the context of figures 3(a) and (b). On the one hand, our data clearly demonstrate that there are two distinguishable optoelectronic mechanisms inside and outside the 2DEG; by specific dependences versus magnetic field (figure 4) and phase (figure 3). Hereby, the dip as seen in figures 3(a) and (b) can be explained. On the other hand, the exciting laser light is scattered on the step of the mesa as can be seen by the reflectance map in figure 2(a). In our understanding, this scattering helped us to detect the differences in optoelectronic response inside and outside of the 2DEG because it can also explain the dip.

The solid white lines in figure 4 indicate the position of the incompressible strips as calculated from equation (2). For all resolved filling factors, the dominant photocurrent occurs for slightly larger magnetic fields than the white lines. This indicates that the photocurrent is carried by the outermost compressible strip of the 2DEG. We note, however, that the excitation of higher, unoccupied Landau levels cannot be neglected for two reasons [50]. First, the width of the incompressible stripes is on the order of 200–300 nm [18, 49], which is below the spatial resolution of our confocal set-up. Second, the calculated Landau-level spacing is $\hbar\omega_c = 1.8\ \mathrm{meV\ T^{-1}} \cdot B$, resulting in 2.7 meV at $\nu = 4$, which is less than the laser linewidth (8 meV). For instance, for lower magnetic fields, we cannot resolve the compressible/incompressible regions due to the limited resolution of our experiment. Therefore, a possible route to better resolve the edge states by the presented scanning photocurrent spectroscopy would be to start with a 2DEG with a larger electron density, such that experimentally applied B would be larger for the lowest Landau-levels. Such a high-magnetic field regime may also allow to resolve the spin transport in the edge states exploiting the selection rules of the optical excitation in GaAs quantum wells in combination with the spin polarization of the one-dimensional subbands of the QPC [51–54].

6. Conclusions

In summary, we use a QPC as a local photocurrent detector to map the propagation of photogenerated charge carriers in a GaAs-based 2DEG at high magnetic fields. We find a photocurrent response at the lateral edges of the 2DEG with a longitudinal extension of several tens of micrometers. The length significantly exceeds the electron mean free path at zero magnetic field. Our results are consistent with photogenerated electrons being injected directly into quantum Hall edge channels. We find an additional optoelectronic response which we explain by charge carriers photogenerated in the vicinity of an edge state which capacitively influence the optoelectronic transport through it. Our work demonstrates that QPCs can be exploited to contact and read-out the optoelectronic transport through edge channels.

Acknowledgments

We thank K-D Hof for initial experiments and discussions. We acknowledge the Deutsche Forschungsgemeinschaft (DFG) for financial support by project HO 3324/4 within SPP 1285 and project HO332/8 within SPP 1666. Three (two) of us AWH, (DS, and WW) thank the DFG for financial support within the collaborative research centers SFB 631 (and 689).

References

[1] Klitzing K V, Dorda G and Pepper M 1980 *Phys. Rev. Lett.* **45** 494
[2] Aoki H 1987 *Rep. Prog. Phys.* **50** 655–730
[3] Yennie D R 1987 *Rev. Mod. Phys.* **59** 781–824
[4] Halperin B I 1982 *Phys. Rev.* B **25** 2185
[5] Büttiker M 1988 *Phys. Rev.* B **38** 9375
[6] Trugman S A 1983 *Phys. Rev.* B **27** 7539–46
[7] Woltjer R, Eppenga R, Mooren J, Timmering C E and André J P 1986 *Europhys. Lett.* **2** 149
[8] Chklovskii D B, Shklovskii B I and Glazman L I 1992 *Phys. Rev.* B **46** 4026
[9] Shashkin A A, Kent A J, Harrison P A, Eaves L and Henini M 1994 *Phys. Rev.* B **49** 5379–85
[10] van Haren R J F, Blom F A P and Wolter J H 1995 *Phys. Rev. Lett.* **74** 1198–201
[11] Shashkin A A, Kent A J, Owers-Bradley J R, Cross A J, Hawker P and Henini M 1997 *Phys. Rev. Lett.* **79** 5114–7
[12] McCormick K L, Woodside M T, Huang M, Wu M, McEuen P L, Duruoz C and Harris J S 1999 *Phys. Rev.* B **59** 4654–7
[13] Weitz P, Ahlswede E, Weis J, Klitzing K V and Eberl K 2000 *Physica* E **6** 247–50
[14] Ahlswede E, Weitz P, Weis J, Klitzing K V and Eberl K 2001 *Physica* B **298** 562–6

[15] Baumgartner A, Ihn T, Ensslin K, Maranowski K and Gossard A C 2007 *Phys. Rev.* B **76** 085316
[16] Kozikov A A, Steinacher R, Rössler C, Ihn T, Ensslin K, Reichl C and Wegscheider W 2014 *New J. Phys.* **16** 053031
[17] Suddards M E, Baumgartner A, Mellor C J and Henini M 2008 *Physica* E **40** 1548–50
[18] Suddards M E, Baumgartner A, Henini M and Mellor C J 2012 *New J. Phys.* **14** 083015
[19] Wei Y Y, Weis J, Klitzing K V and Eberl K 1998 *Phys. Rev. Lett.* **81** 1674
[20] Yacoby A, Hess H F, Fulton T A, Pfeiffer L N and West K W 1999 *Solid State Commun.* **111** 1–13
[21] Finkelstein G, Glicofridis P I, Ashoori R C and Shayegan M 2000 *Science* **289** 90–4
[22] Zhitenev N B, Fulton T A, Yacoby A, Hess H F, Pfeiffer L N and West K W 2000 *Nature* **404** 473–6
[23] Hashimoto K, Sohrmann C, Wiebe J, Inaoka T, Meier F, Hirayama Y, Römer R A, Wiesendanger R and Morgenstern M 2008 *Phys. Rev. Lett.* **101** 256802
[24] Lai K, Kundhikanjana W, Kelly M A, Shen Z-X, Shabani J and Shayegan M 2011 *Phys. Rev. Lett.* **107** 176809
[25] Venkatachalam V, Hart S, Pfeiffer L, West K and Yacoby A 2012 *Nat. Phys.* **8** 676–81
[26] Altimiras C, le Sueur H, Gennser U, Anthore A, Cavanna A, Mailly D and Pierre F 2012 *Phys. Rev. Lett.* **109** 026803
[27] Paradiso N, Heun S, Roddaro S, Sorba L, Beltram F, Biasiol G, Pfeiffer L N and West K W 2012 *Phys. Rev. Lett.* **108** 246801
[28] Pascher N, Rössler C, Ihn T, Ensslin K, Reichl C and Wegscheider W 2014 *Phys. Rev.* X **4** 011014
[29] Stallhofer M, Kastl C, Brändlein M, Karnetzky C, Schuh D, Wegscheider W and Holleitner A W 2012 *Phys. Rev.* B **86** 115313
[30] Stallhofer M, Kastl C, Brändlein M, Schuh D, Wegscheider W and Holleitner A W 2012 *Phys. Rev.* B **86** 115315
[31] König M, Wiedmann S, Brüne C, Roth A, Buhmann H, Molenkamp L W, Qi X-L and Zhang S-C 2007 *Science* **318** 766
[32] Murakami S 2007 *New J. Phys.* **9** 356
[33] Nowack K C *et al* 2013 *Nat. Mater.* **12** 787
[34] Kristensen A, Jensen J B, Zaffalon M, Sorensen C B, Reimann S M, Lindelof P E, Michel M and Forchel A 1998 *J. Appl. Phys.* **83** 607
[35] Hof K-D, Rössler C, Manus S, Kotthaus J P, Holleitner A W, Schuh D and Wegscheider W 2008 *Phys. Rev.* B **78** 115325
[36] Buchholz S S, Sternemann E, Chiatti O, Reuter D, Wieck A D and Fischer S F 2012 *Phys. Rev.* B **85** 235301
[37] Poggio M, Jura M P, Degen C L, Topinka M A, Mamin H J, Goldhaber-Gordon D and Rugar D 2008 *Nat. Phys.* **4** 635–8
[38] Hof K-D, Kaiser F J, Stallhofer M, Schuh D, Wegscheider W, Hänggi P, Kohler S, Kotthaus J P and Holleitner A W 2010 *Nano Lett.* **10** 3836
[39] Hof K-D, Rössler C, Wegscheider W, Ludwig S and Holleitner A W 2008 *Physica* E **40** 1739
[40] Rössler C, Hof K-D, Manus S, Ludwig S, Kotthaus J P, Simon J, Holleitner A W, Schuh D and Wegscheider W 2008 *Appl. Phys. Lett.* **93** 071107
[41] Zimmermann S, Wixforth A, Kotthaus J P, Wegscheider W and Bichler M 1999 *Science* **283** 1292
[42] Wharam D A, Thornton T J, Newbury R, Pepper M, Ahmed H, Frost J E F, Hasko D G, Peacock D C, Ritchie D A and Jones G A C 1988 *J. Phys. C: Solid State Phys.* **21** 209–14
[43] van Wees B J, Kouwenhoven L P, van der Marel D, von Houten H and Beenakker C W J 1988 *Phys. Rev. Lett.* **60** 848–50
[44] Smith T P, Goldberg B B, Heiblum M and Stiles P J 1985 *Phys. Rev.* B **32** 2696–9
[45] Mosser V, Weiss D, Klitzing K V, Ploog K and Weimann G 1986 *Solid State Commun.* **58** 5–7
[46] Jagdeep S 1999 *Ultrafast Spectroscopy of Semiconductors and Semiconductor Nanostructures* (Berlin: Springer)
[47] Siddiki A and Gerhardts R R 2004 *Phys. Rev.* B **70** 195335
[48] Grant R W, Waldrop J R, Kowalczyk S P and Kraut E A 1981 *J. Vac. Sci. Technol.* **19** 477
[49] Steele G A, Ashoori R C, Pfeiffer L N and West K W 2005 *Phys. Rev. Lett.* **95** 136804
[50] Ito H, Furuya K, Shibata Y, Kashiwaya S, Yamaguchi M, Akazaki T, Tamura H, Ootuka Y and Nomura S 2011 *Phys. Rev. Lett.* **107** 256803
[51] Diehl H *et al* 2007 *New J. Phys.* **9** 349
[52] Bauer F, Heyder J, Schubert E, Borowsky D, Taubert D, Bruognolo B, Schuh D, Wegscheider W, von Delft J and Ludwig S 2013 *Nature* **501** 73
[53] Bhandari N, Dutta M, Charles J, Newrock R S, Cahay M and Herbert S T 2013 *Adv. Nat. Sci.: Nanosci. Nanotechnol.* **4** 013002
[54] Karzig T, Levchenko A, Glazman L and Oppen F V 2012 *New J. Phys.* **14** 105009